Supplementary Information

Electron Transmission Matrix and Anion Regulation Strategy-Derived Oxygen-Deficient δ-MnO_2 for a High-Rate and Long-Life Aqueous Zinc-Ion Battery

Junyi Yin,[a] *Hui Yang,*[b,c] *Zihan Gan,*[a] *Yuan Gao,*[a] *Xiang Feng,*[a] *Minghui Wang,*[a] *Gaixiu Yang,*[b,c] *Yonghong Cheng*[a]* *and Xin Xu*[a]*

[a] State Key Laboratory of Electrical Insulation and Power Equipment, School of Electrical Engineering, Xi'an Jiaotong University, Xi'an 710049, China

[b] School of Engineering Science, University of Science and Technology of China, Hefei 230026, China.

[c] CAS Key Laboratory of Renewable Energy Guangdong Provincial Key Laboratory of New and Renewable Energy Research and Development, Guangzhou Institute of Energy Conversion, Chinese Academy of Sciences, Guangzhou 510640, China.

*Corresponding authors.

E-mail addresses: cyh@xjtu.edu.cn (Y. Cheng), xu.xin@xjtu.edu.cn (X. Xu).

Experimental Section

Material Synthesis

Synthesis of hollow carbon microtubes (HCMTs): HCMTs was synthesized via pyrolysis reaction. Energy grass, dicyandiamide, and ferric chloride are mixed evenly in a ratio of 1:1:0.16. The mixture was stirred in ethanol solution at 500 rpm for 8h. Then the mixture solution is dried at 55 °C and ground to powder form to obtain the pyrolytic precursor. The pyrolysis process is carried out in tube furnaces, and the reaction procedure consists of heating process from room temperature to 800 °C with rate of 20 °C min^{-1} and insulation process at 800 °C. When the pyrolysis process is completed, the products are taken out and subjected to acid and water washing in turn. After that the products are dried to a constant weight at 50 °C and collected.

Synthesis of Pristine MnO_2. 500 mg of $KMnO_4$ and 80 ml of DI water were mixed to form a uniform suspension. The mixture was stirred and sonicated for 30 minutes and transferred to a 100 ml Teflon-lined autoclave. The autoclave was kept in an oven at 180 °C for 12 h and the brownish production was collected by high speed centrifugation at 8000 rpm, washed with DI water and ethanol for several times and dried in an oven at 80 °C to obtain the final product.

Synthesis of N-MnO_2. 500 mg of $KMnO_4$, 15 mg Urea and 80 ml of DI water were mixed to form a uniform suspension. The mixture was stirred and sonicated for 30 minutes and transferred to a 100 ml Teflon-lined autoclave. The autoclave was kept in an oven at 180 °C for 12 h and the brownish production was collected by high speed

centrifugation at 8000 rpm, washed with DI water and ethanol for several times and dried in an oven at 80 °C to obtain the final product.

Synthesis of N-MnO_2@HCMTs. 30 mg of HCMTs, 500 mg of $KMnO_4$, 15 mg Urea and 80 ml of DI water were mixed to form a uniform suspension. The mixture was stirred and sonicated for 30 minutes and transferred to a 100 ml Teflon-lined autoclave. The autoclave was kept in an oven at 180 °C for 12 h and the brownish production was collected by high speed centrifugation at 8000 rpm, washed with DI water and ethanol for several times and dried in an oven at 80 °C to obtain the final product.

Synthesis of PAM/$ZnSO_4$-$MnSO_4$ gel: 5.815 g acrylamide, 28.6 mg sodium persulfate, 3.5 mg N, N-methylenebisacrylamide and 0.718 g sodium alginate were added together and stirred for several hours to obtain uniform mixture. Then the mixture was polymerized for four hours in a 60 ℃ vacuum oven. After that, the product was immersed into 2 M $ZnSO_4$ and 0.1 M $MnSO_4$ solution to obtain the PAM/$ZnSO_4$-$MnSO_4$ gel.

Materials Characterization

Field Emission Scanning Electron Microscope (FESEM; ZEISS, Gemini 500) and Field Emission Transmission Electron Microscope (FETEM; Talos F200X) coupled with energy dispersive X-ray spectroscopy (EDS) was used to acquire the morphology of materials, elemental mapping images and selected area electron diffraction (SAED) patterns. X-ray diffraction (XRD) analysis was recorded by Bruker D8 Advance with a Cu Kα radiation (λ=1.54184 Å). X-ray photoelectron spectroscopy (XPS) analysis were acquired by the AXIS ULtrabld. Raman spectra were collected by a Renishaw Raman

RE01 utilizing a 633 nm laser. Thermogravimetric Analysis (TGA; METTLER TOLEDO TGA/DSC3+) were carried out with a flow of air at a heating rate of 10 °C min^{-1} from room temperature to 600 °C. The nitrogen adsorption-desorption isotherms and pore-size distributions of the samples were obtained from Automatic physical adsorption instrument (ASAP 2020 Plus HD88).

Electrochemical Measurements

The coin cells (CR 2025) were assembled in the air atmosphere. The working electrode was composed of 70% as-prepared active material, 20% conductive agent (super P, Timcal) and 10% polymer binder (PVDF, Macklin). The mass loading of the active materials is about 1.0 mg cm^{-2}. The electrolyte used was 2 M $ZnSO_4$ and 0.1 M $MnSO_4$ aqueous solution. The counter electrode and reference electrode are both served by Zn foil only. The galvanostatic charge-discharge (GCD) and Galvanostatic Intermittent Titration Technique (GITT) tests were conducted on the NEWARE battery tester. Cyclic voltammetry (CV) test was performed at a scan rate from 0.8 to 1.8 mV s^{-1} using an electrochemical workstation (CHI 1040C, CH Instruments, Ins). The Nyquist plots was obtained from CHI 760E (CH Instruments, Ins) with the frequency ranges from 0.01 Hz to 100 MHz.

Calculation of the Diffusion Coefficients of Zinc Ions

The diffusion coefficients of zinc ions (D_{Zn}^{2+}) in NCMO and pristine MnO_2 are calculated based on Equation 1:

$$D_{Zn}^{2+}=4(n_m V_m)^2 S^{-2}(\pi\tau)^{-1}(\Delta E_s)^2(\Delta E_\tau)^{-2} \quad (1)$$

in which τ (s) represents the constant current pulse time, n_m (g mol^{-1}) and V_m (cm^3 mol^{-1}) are assigned to the number of moles and the molar volume of the active materials, and S (cm^2) is the contact area of electrode. ΔE_s and ΔE_t denote the potential change triggered by the pulse and constant current charge–discharge, respectively. A current density of 100 mA g^{-1} is applied to the cells with τ=10 min and then stood for 600 s without current impulse.

Supplementary Figures:

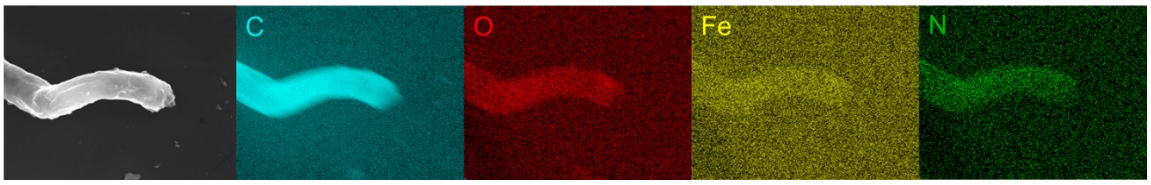

Figure S1. Element mapping of HCMTs sample.

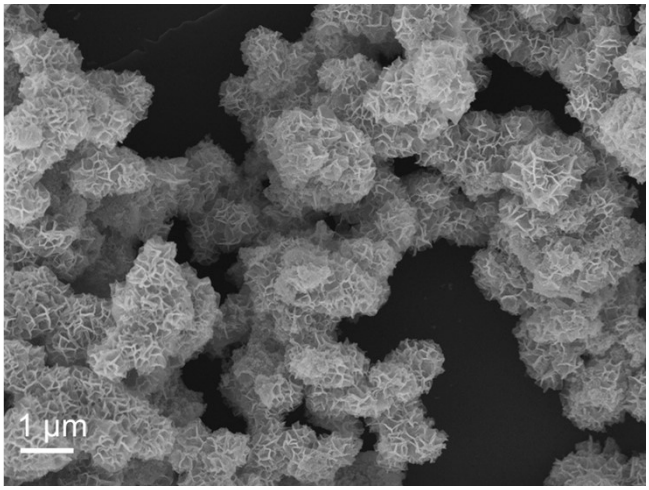

Figure S2. FESEM images of N-MnO_2 material.

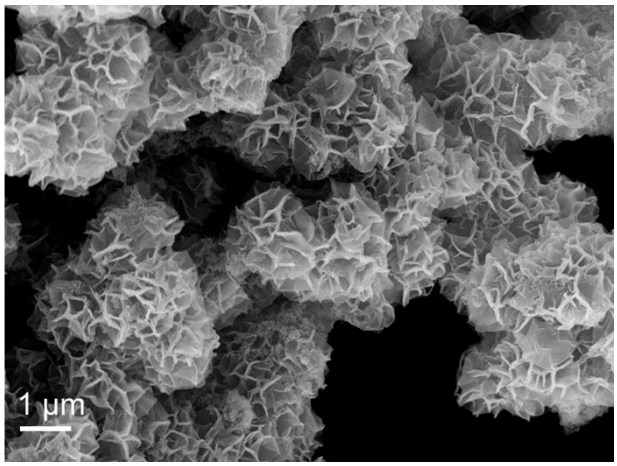

Figure S3. FESEM images of pristine MnO_2 material.

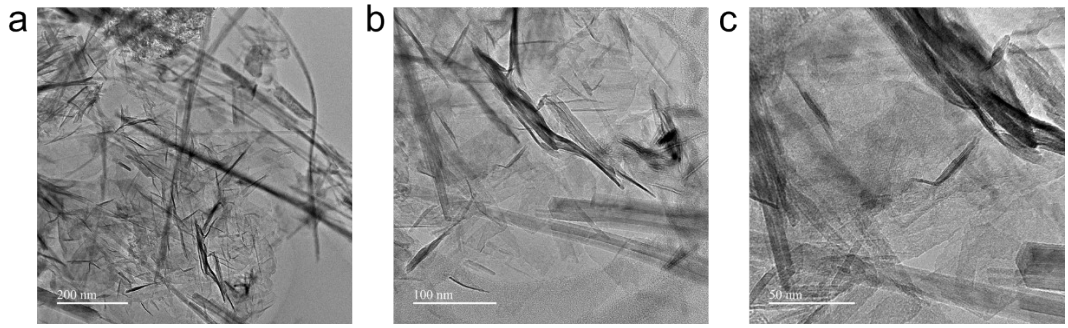

Figure S4. Images of N-MnO_2@HCMTs with different scales. Scale bar: (a) 200 nm; (b) 100 nm; (c) 50 nm.

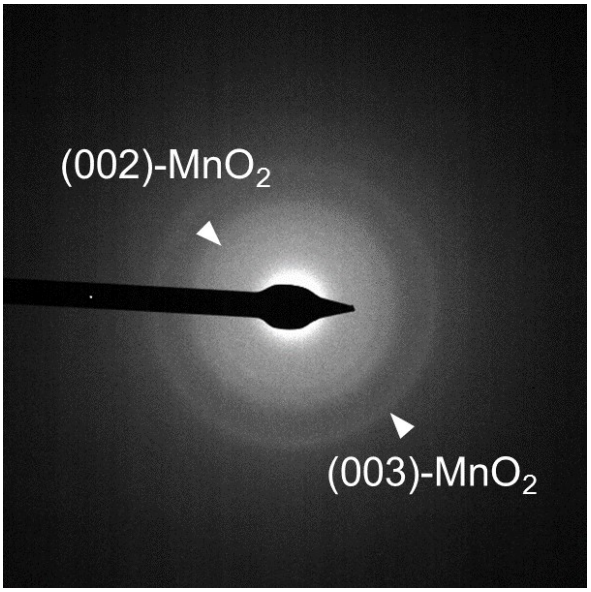

Figure S5. SAED pattern of N-MnO_2@HCMTs.

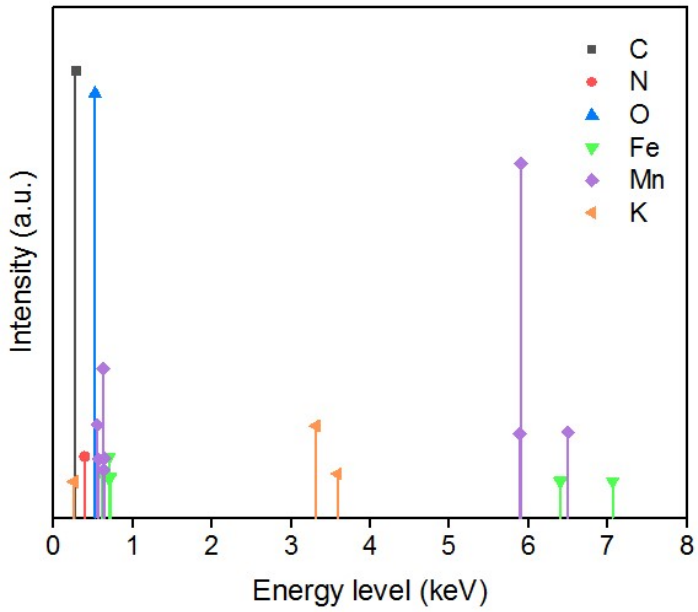

Figure S6. Energy dispersive X-ray spectroscopy of N-MnO_2@HCMTs.

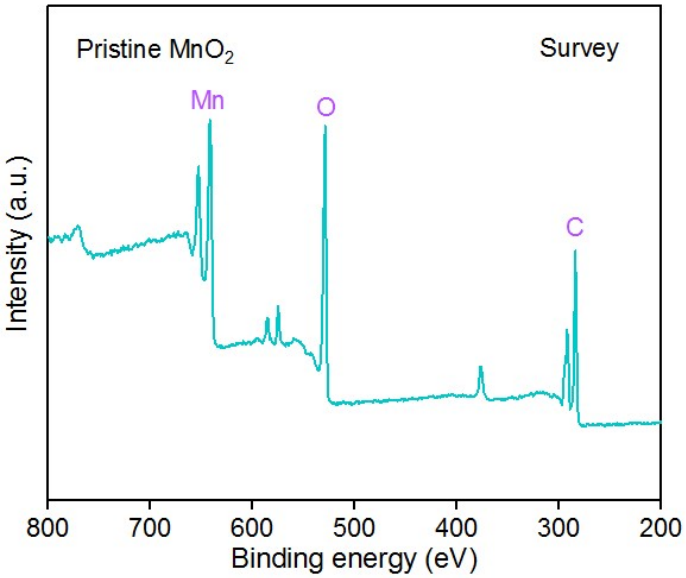

Figure S7. XPS spectra of pristine MnO_2.

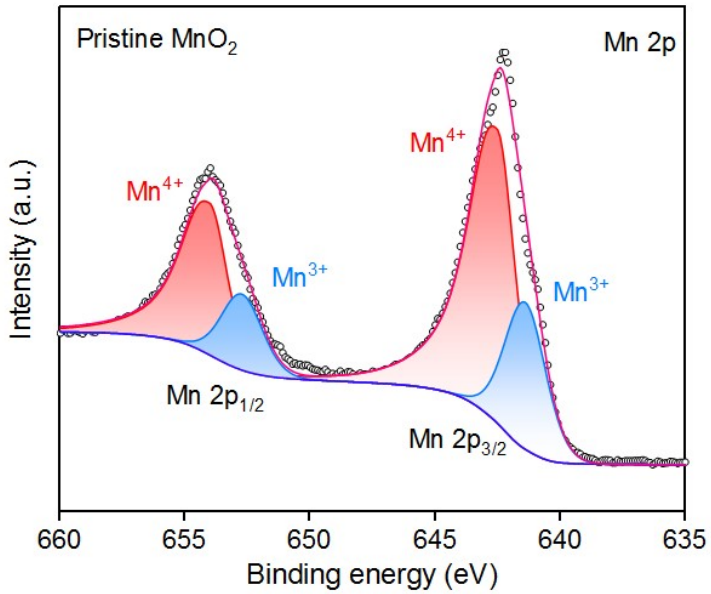

Figure S8. High-resolution XPS spectra of Mn 2p in pristine MnO_2.

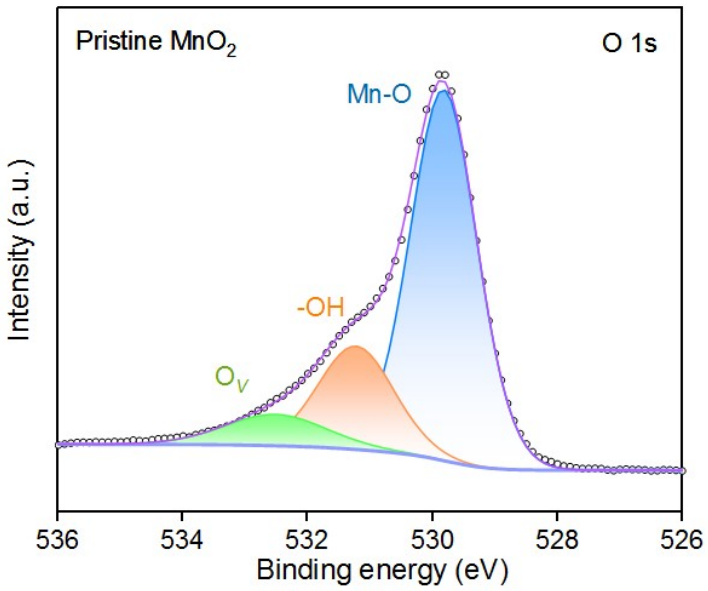

Figure S9. High-resolution XPS spectra of O 1s in pristine MnO_2.

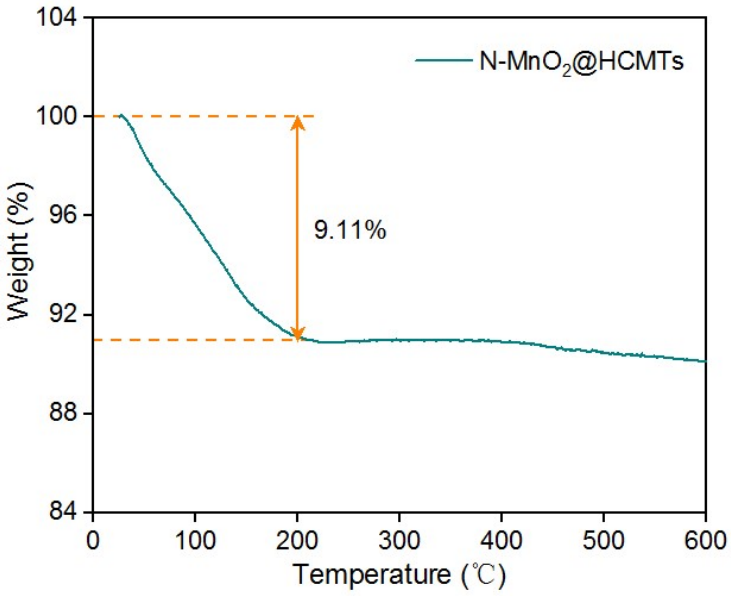

Figure S10. TGA curves of N-MnO_2@HCMTs samples.

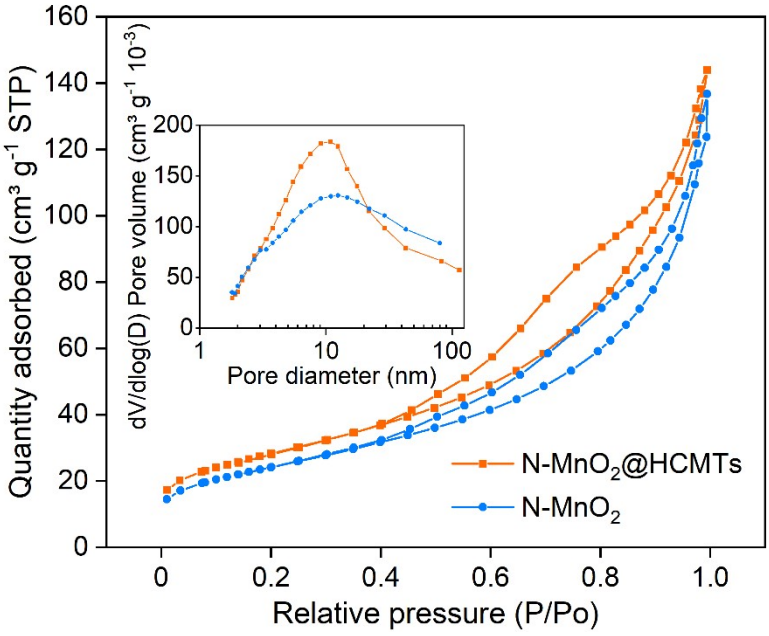

Figure S11. N_2 adsorption-desorption isotherms (inset: the pore-size distributions) of N-MnO_2@HCMTs and N-MnO_2 sample.

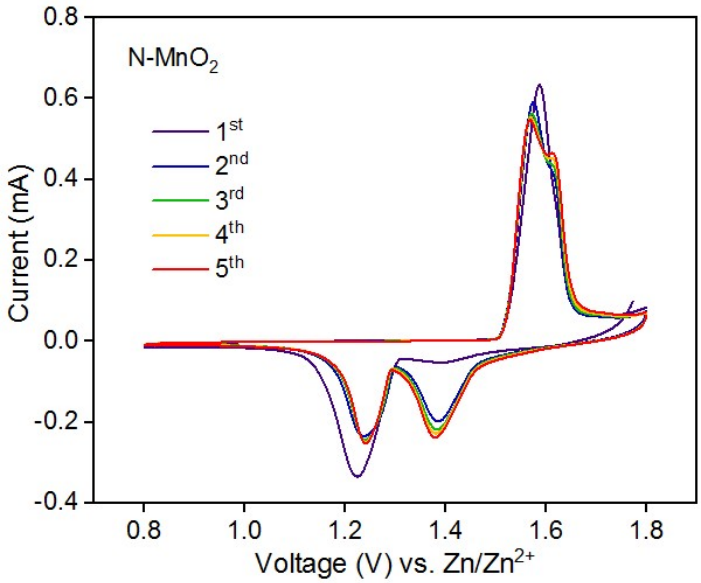

Figure S12. Initial five CV curves of N-MnO_2.

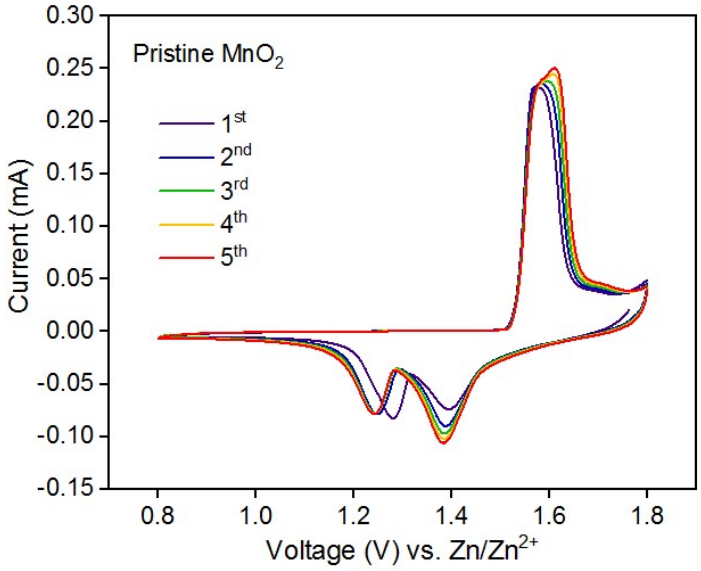

Figure S13. Initial five CV curves of pristine MnO_2.

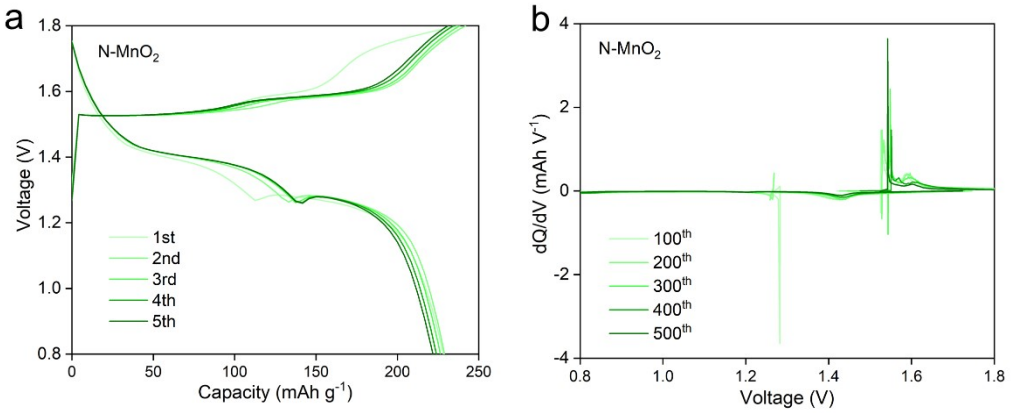

Figure S14. a) GCD profiles and b) dQ/dV curves of N-MnO_2 samples.

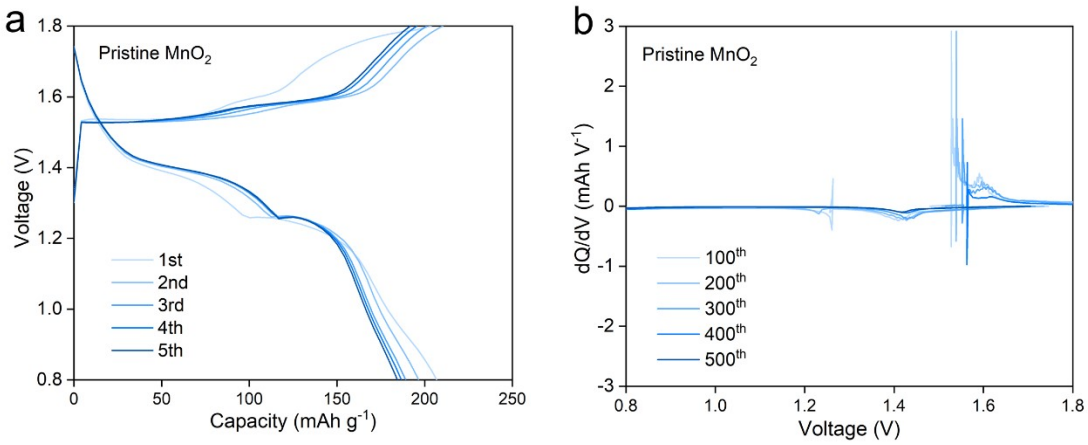

Figure S15. a) GCD profiles and b) dQ/dV curves of pristine MnO_2 samples.

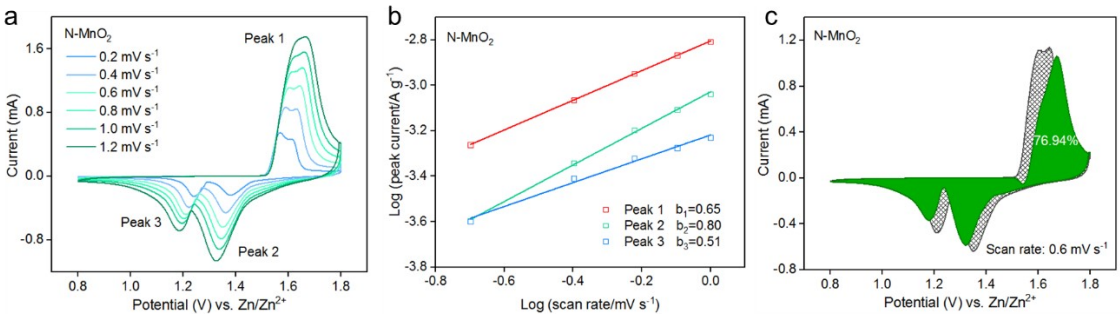

Figure S16. Quantitative analysis of Zn^{2+} storage kinetics for N-MnO_2 cathode. a) CV curves of N-MnO_2 cathode. b) Plots of the logarithm peak current vs. the logarithm scan rate for N-MnO_2 cathode. c) Separation of capacitive and diffusion-controlled currents of N-MnO_2 cathode at 0.6 mV s^{-1}.

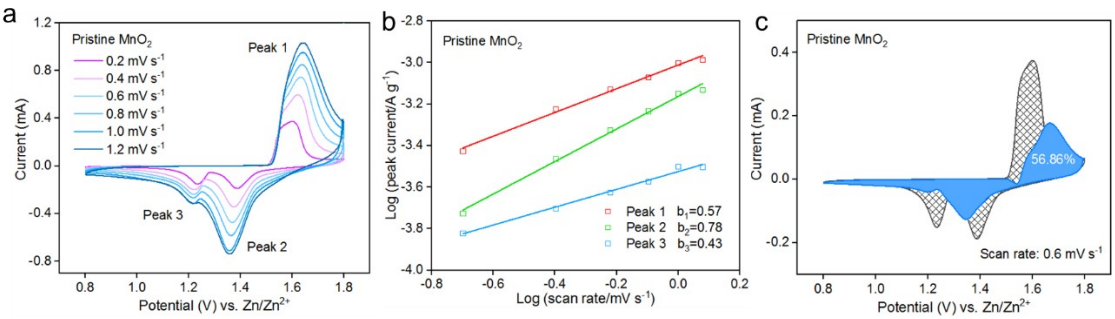

Figure S17. Quantitative analysis of Zn^{2+} storage kinetics for pristine MnO_2 cathode. a) CV curves of N-MnO_2 cathode. b) Plots of the logarithm peak current vs. the logarithm scan rate for pristine MnO_2 cathode. c) Separation of capacitive and diffusion-controlled currents of pristine MnO_2 cathode at 0.6 mV s^{-1}.

Table S1. The fitting values of impedance parameters of N-MnO_2@HCMTs, N-MnO_2 and pristine MnO_2.

Electrode	R_Ω (Ω)	R_{ct} (Ω)	w (S $s^{1/2}$)		
			R	T	P
N-MnO_2@HCMTs	1.943	13.79	104.6	0.343	0.247
N-MnO_2	1.40	11.68	140.3	0.854	0.323
pristine MnO_2	2.497	904.3	3955	2404	0.403

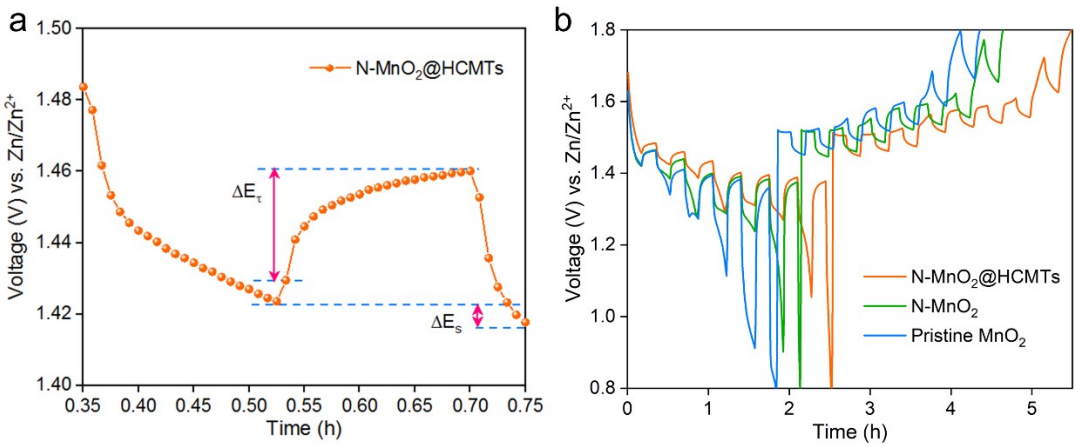

Figure S18. a) The detailed GITT diagram with a single current pulse for 10 min followed by an open-circuit for 600 s. b) GITT curves of three samples.

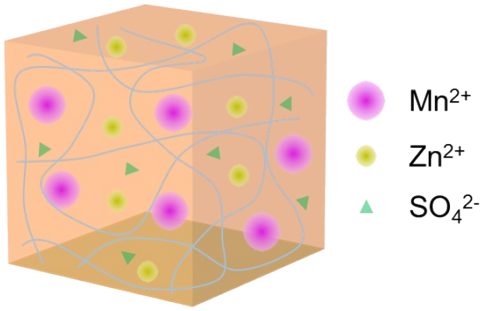

Figure S19. The illustration of quasi-solid-state PAM/$ZnSO_4$-$MnSO_4$ gel.

Figure S20. The mechanical flexibility test of quasi-solid-state gel. Twisting (a), and stretching (b-c).

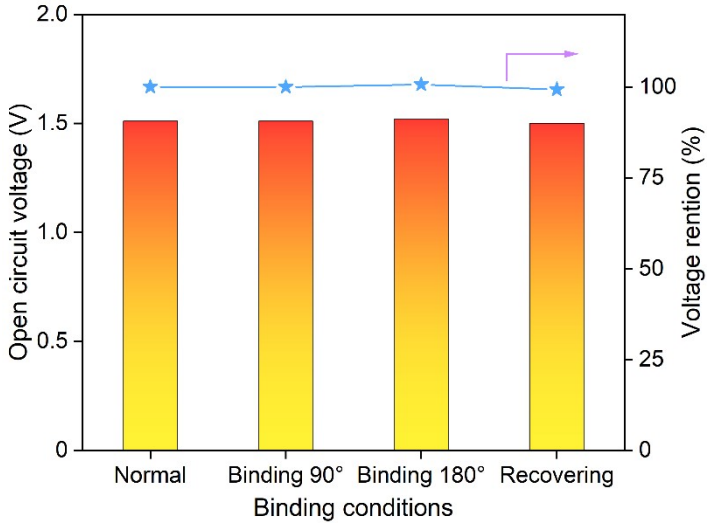

Figure S21. The open voltages of flexible quasi-solid-state N-MnO_2@HCMTs//Zn cell at different states.

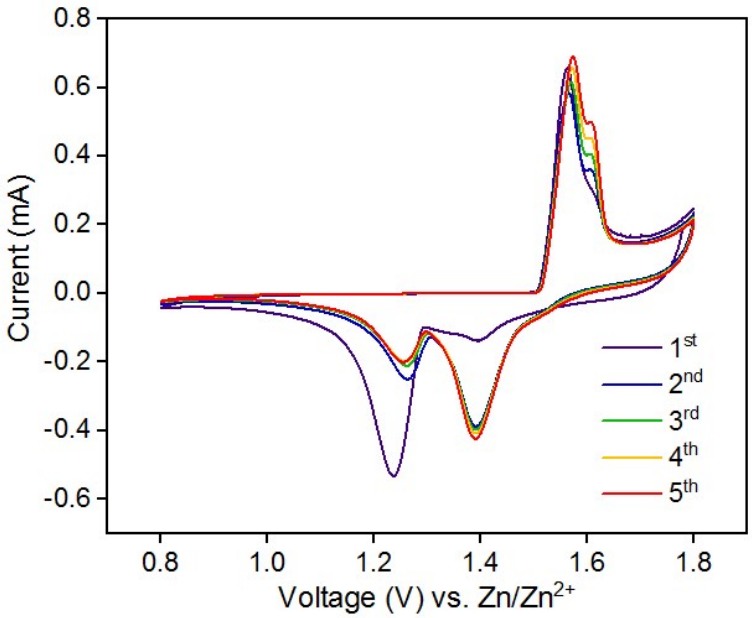

Figure S22. The initial five CV curves of N-MnO_2@HCMTs//Zn cell (scan rate: 0.2 mV s^{-1}).

Table S2. The fitting values of impedance parameters of N-MnO_2@HCMTs//Zn battery at different bending states.

Electrode	R_Ω (Ω)	R_{ct} (Ω)	w (S $s^{1/2}$)		
			R	T	P
Normal	3.264	42.76	73.48	1.686	0.366
Bending 90°	3.262	27.51	79.24	1.725	0.365
Bending 180°	3.127	23.16	59.94	1.40	0.367
Recovering	3.195	23.09	74.29	1.607	0.366

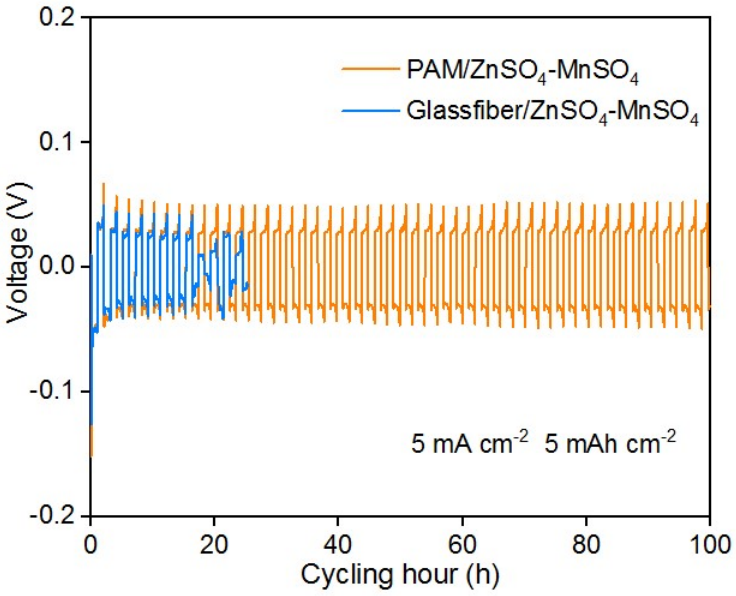

Figure S23. Comparison of cycling performances of Zn//Zn symmetric cells under 5 mA cm^{-2} and 5 mAh cm^{-2}.

Figure S24. The open voltage of two quasi-solid-state cells linked in series.

Table S3. Performance comparison for reported representative Mn-based aqueous ZIBs and flexible ZIBs with our N-MnO_2@HCMTs flexible ZIBs.

Cathodes	Capacity	Cycling performance	Refs.
N-MnO_{1-x}@N-C[1]	126 mAh g^{-} at 5 A g^{-1}	89% capacity retention after 2000 cycles at 2 A g^{-1}	*Nano Res.,* 2022, 15, 8603–8612.
S-MnO_2[2]	324 mAh g^{-1} at 200 mA g^{-1}	95% capacity retention after 100 cycles at 200 mA g^{-1}	*Energy Storage Mater.*, 2022, 47, 424-433.
Ce-MnO_2@CC[3]	105.1 mAh g^{-1} at 2 A g^{-1}	~100% capacity retention after 450 cycles at 100 mA g^{-1}	*Chem. Eng. J.*, 2022, 431, 133387.
$K_{0.27}MnO_2 \cdot 0.54H_2O$ [4]	280 mAh g^{-1} at 100 mA g^{-1}	86% capacity retention after 100 cycles at 100 mA g^{-1}	*Adv. Energy Mater.*, 2021, 2101287.
$Na_{0.55}Mn_2O_4 \cdot 1.5H_2O$ [5]	367.5 mAh g^{-1} at 0.65 C	10000 cycles at 6.5 C with a capacity decay rate of 0.007% per cycle	*Energy Storage Mater.*, 2021, 38, 299–308.
β-MnO_2 [6]	283 mAh g^{-1} at 100 mA g^{-1}	85% capacity retention after 150 cycles at a 0.5 A g^{-1}	*J. Mater. Chem. A*, 2021,9, 17211-17222.
K-MnO_d [7]	203 mAh g^{-1} at 2 A g^{-1}	81.3% capacity retention after 2500 cycles at a 2 A g^{-1}	*J. Mater. Chem. A*, 2021, 9, 15637–15647.
Co-Mn_3O_4 [8]	220 mAh g^{-1} at 100 mA g^{-1}	71% capacity retention after 1000 cycles at 4 A g^{-1}	*Adv. Energy Mater.*, 2020, 2003203.
O_d-Mn_3O_4@C NA/CC [9]	396.2 mAh g^{-1} at 200 mA g^{-1}	95.7% capacity retention after 12000 cycles at 5 A g^{-1}	*Adv. Energy Mater.*, 2020, 10, 2001050.
N-CNSs@MnO_2 [10]	303.7 mAh g^{-1} at 200 mA g^{-1}	91.6% capacity retention after 1800 cycles at 2 A g^{-1}	*Energy Storage Mater.,* 2020, 29, 52–59.
$Ca_{0.28}MnO_2 \cdot 5H_2O$ [11]	298 mAh g^{-1} at 175 mA g^{-1}	100.9 mAh g^{-1} after 5000 cycles at 3500 mA g^{-1}	*Small*, 2020, 16, 2000597.
La-Ca doped MnO_2 [12]	297 mAh g^{-1} at 200 mA g^{-1}	76.8% capacity retention after 200 cycles	*J. Mater. Chem. A*, 2020, 8, 11642-11648
$Na_{0.44}Mn_2O_4 \cdot 1.5H_2O$[13]	278 mAh g^{-1} at 1 C	98% capacity retention after 10000 cycles at 20 C	*ACS Nano*, 2019, 13, 10643-10652.
Zn-stabilized MnO_2 [14]	124 mAh g^{-1} at 3.0 A g^{-1}	358 mAh g^{-1} at 0.3 A g^{-1} after 100 cycles	*J. Mater. Chem. A,* 2019, 7, 13727.
N-MnO_2@HCMTs	277 mAh g^{-1} at 10 A g^{-1}	87 % capacity retention after 5000 cycles at 10 A g^{-1}	*This work*

References

[1] H. Luo, L. P. Wang, P. H. Ren, J. H. Jian, X. Liu, C. J. Niu, D. L. Chao, *Nano Res.* **2022**, 15, 8603.

[2] Y. J. Zhao, P. J. Zhang, J. R. Liang, X. Y. Xia, L. T. Ren, L. Song, W. Liu, X. M. Sun, *Energy Storage Mater.* **2022**, 47, 424.

[3] Y. Y. Song, J. M. Li, R. Qiao, X. Dai, W. T. Jing, J. X. Song, Y. Z. Chen, S. W. Guo, J. J. Sun, Q. Tan, Y. N. Liu, *Chem. Eng. J.* **2022**, 431, 10, 133387.

[4] L. Liu, Y. C. Wu, L. Huang, K. Liu, B. Duployer, P. Rozier, P. L. Taberna, P. Simon, *Adv. Energy Mater.* **2021**, 11, 2101287.

[5] Y. Xu, J. Zhu, J. Feng, Y. Wang, X. Wu, P. Ma, X. Zhang, G. Wang, X. Yan, *Energy Storage Mater.* **2021**, 38, 299.

[6] S. Kim, B.-R. Koo, Y.-R. Jo, H.-R. An, Y.-G. Lee, C. Huang, G.-H. An, *J. Mater. Chem. A* **2021**, 9, 17211.

[7] K. Han, F. An, F. Yan, H. Chen, Q. Wan, Y. Liu, P. Li, X. Qu, *J. Mater. Chem. A* **2021**, 9, 15637.

[8] J. Ji, H. Wan, B. Zhang, C. Wang, Y. Gan, Q. Tan, N. Wang, J. Yao, Z. Zheng, P. Liang, J. Zhang, H. Wang, L. Tao, Y. Wang, D. Chao, H. Wang, *Adv. Energy Mater.* **2020**, 11, 2003203.

[9] Q. Tan, X. Li, B. Zhang, X. Chen, Y. Tian, H. Wan, L. Zhang, L. Miao, C. Wang, Y. Gan, J. Jiang, Y. Wang, H. Wang, *Adv. Energy Mater.* **2020**, 10, 2001050.

[10] Y. Zhang, S. Deng, Y. Li, B. Liu, G. Pan, Q. Liu, X. Wang, X. Xia, J. Tu, *Energy Storage Mater.* **2020**, 29, 52.

[11] T. Sun, Q. Nian, S. Zheng, J. Shi, Z. Tao, *Small* **2020**, 16, 2000597.

[12] M. Zhang, W. Wu, J. Luo, H. Zhang, J. Liu, X. Liu, Y. Yang, X. Lu, *J. Mater. Chem. A* **2020**, 8, 11642.

[13] D. Wang, L. Wang, G. Liang, H. Li, Z. Liu, Z. Tang, J. Liang, C. Zhi, *ACS Nano* **2019**, 13, 10643.

[14] J. Wang, J.-G. Wang, H. Liu, C. Wei, F. Kang, *J. Mater. Chem. A* **2019**, 7, 13727.